Range–Angle Processing for Target Detection in Joint MIMO-OFDM Communications and Sensing

Sahan Damith Liyanaarachchi, Carlos Baquero Barneto, Taneli Riihonen, Mikko Heino, and Mikko Valkama
Electrical Engineering, Faculty of Information Technology and Communication Sciences, Tampere University, Finland
Email: {sahan.liyanaarachchi, carlos.baquerobarneto, taneli.riihonen, mikko.heino, mikko.valkama}@tuni.fi

***Abstract*—Utilizing multiple-input multiple-output (MIMO) communication systems to jointly perform sensing will be a key ingredient in future mobile networks. To accommodate this, here we propose a signal processing approach for target detection in hybrid MIMO orthogonal frequency-division multiplexing communication systems. We utilize multiple transmit beams for communication users, while an additional beam is used simultaneously to sense the environment. Then, the reflections from the targets due to the transmitted streams are utilized at the MIMO receiver to obtain the range–angle map corresponding to the environment. Simulations depict that targets can be detected reliably using this approach. Moreover, it showcases that MIMO processing allows differentiating between very close targets in the angular domain, demonstrating the achievable super-resolution.**

***Index Terms*—Joint communication and sensing, MIMO, MUSIC, OFDM, radar.**

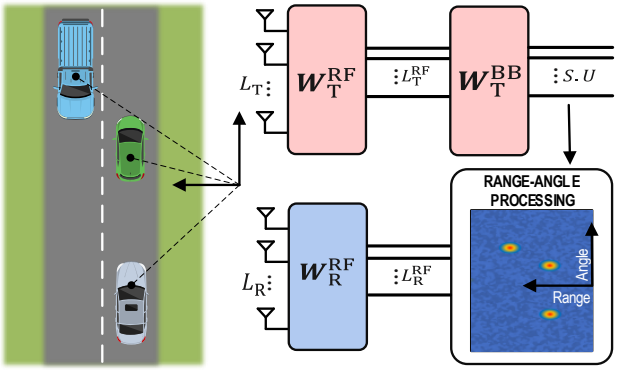

Fig. 1. The considered MIMO-OFDM JCAS system.

I. Introduction

The separate operation of communication and sensing systems has caused spectrum scarcity and mutual interference. Joint communication and sensing (JCAS) systems have emerged as a solution for these challenges where they are designed for efficient resource allocation [1], and many applications have benefited from the joint functioning, e.g., automotive radar, cellular networks, and indoor mapping [2].

Mobile communication systems are moving to operate around mm-wave frequencies to provide increased data rates to the users. However, due to the high attenuation evident in these frequencies, multiple-input multiple-output (MIMO) technology is necessary, which provides high gains through spatial multiplexing and directional beams [3].

Sensing systems can also benefit due to the MIMO operation since they provide more degrees of freedom in radar processing, improving the target detection [4]. Typically in these MIMO radars, the receive (RX) antennas are spaced at a half-wavelength distance, while the transmit (TX) antennas have a much farther separation. Additionally, the signals from different TX antennas are made orthogonal, which allow super-resolution in direction of arrival (DoA) estimation [5]. Thus, the design of MIMO JCAS systems has received increased interest due to these advantages for both communication and sensing functionalities [6].

In this work, we consider performing JCAS in the perspective of a MIMO communication system. Unlike in MIMO radars, the additional constraints on the antenna separation and the orthogonality between the TX antennas' signals cannot be practically implemented in such a system. Therefore, the contribution of this paper is on performing JCAS by also considering these limitations. We adopt a MIMO system with hybrid analog-digital architecture [7], where both the TX and RX antennas are spaced at half-wavelength. Orthogonal frequency-division multiplexing (OFDM) is used as the TX waveform, and the signals are not necessarily orthogonal between different TX antennas. Multiple beams are employed to cater to different users, while a sensing beam is used concurrently to sense the environment. Additionally, the cross-interference between the users is also suppressed.

We then demonstrate a signal processing approach to obtain the range profiles, which are utilized to obtain the angle profiles using multiple signal classification (MUSIC) algorithm [8], thereby constructing the range–angle map of the considered environment. The numerical results indicate that the targets can be reliably observed even if they are spaced very close in the angular domain, indicating that super-resolution can be achieved with the related range–angle processing.

II. System Model

A MIMO-OFDM system is used in this work, as illustrated in Fig. 1, using a hybrid analog-digital architecture. The JCAS system works as a communication TX as well as a radar transceiver. At the TX side, multiple communication links are maintained, while an additional beam is used to sense the environment. The number of antenna elements and radio-frequency (RF) chains (equivalent to the number of subarrays) are given by L_{T} and $L_{\mathrm{T}}^{\mathrm{RF}}$, and L_{R} and $L_{\mathrm{R}}^{\mathrm{RF}}$, for the TX and RX sides, respectively. As the TX waveform, OFDM is utilized, with M symbols, each with N active subcarriers.

Each communication user is assumed to have S streams, and the TX frequency-domain symbols of the u^{th} user at n^{th} subcarrier and m^{th} OFDM symbol are given by $\mathbf{x}_{u,n,m}$, which is of size $S \times 1$, with $n \in [1, N]$, $m \in [1, M]$, and $u \in [1, U]$, where U is the number of communication users. The baseband (BB) weights for the u^{th} user are given by $\mathbf{W}_{\text{T},u}^{\text{BB}}$, which is a matrix of size $L_{\text{T}}^{\text{RF}} \times S$. The TX RF weights are common to all users and are given by the matrix $\mathbf{W}_{\text{T}}^{\text{RF}}$, which is of size $L_{\text{T}} \times L_{\text{T}}^{\text{RF}}$. Then, the frequency-domain symbols at the TX antenna elements are given by

$$\tilde{\mathbf{x}}_{n,m} = \mathbf{W}_{\text{T}}^{\text{RF}} \sum_{u=1}^{U} \mathbf{W}_{\text{T},u}^{\text{BB}} \mathbf{x}_{u,n,m} = \mathbf{W}_{\text{T}}^{\text{RF}} \mathbf{W}_{\text{T}}^{\text{BB}} \mathbf{x}_{n,m}, \tag{1}$$

where $\tilde{\mathbf{x}}_{n,m}$ is of size $L_{\text{T}} \times 1$, and

$$\mathbf{W}_{\text{T}}^{\text{BB}} = \left[\mathbf{W}_{\text{T},1}^{\text{BB}}, \mathbf{W}_{\text{T},2}^{\text{BB}}, \ldots, \mathbf{W}_{\text{T},U}^{\text{BB}}\right], \tag{2}$$

$$\mathbf{x}_{n,m} = \left[\mathbf{x}_{1,n,m}^{T}, \mathbf{x}_{2,n,m}^{T}, \ldots, \mathbf{x}_{U,n,m}^{T}\right]^{T}, \tag{3}$$

which are respectively of sizes $L_{\text{T}}^{\text{RF}} \times (S \cdot U)$ and $(S \cdot U) \times 1$.

A. TX and RX Beamforming

At the TX side, multiple beams are provided for the U communication users at angles denoted by $\theta_{\text{c},u}$, while a sensing beam is used additionally at θ_{r}. We assume that the angles $\theta_{\text{c},u}$ are known by the MIMO transceiver, whereas θ_{r} could be any arbitrary angle. Having a separate sensing beam allows to detect any target at θ_{r}, but since it is not known beforehand, θ_{r} is chosen arbitrarily. Further, the inter-user interference between the communication users is minimized by imposing nulls in the TX beam pattern at other users' directions. To achieve all these requirements, BB and RF beamforming weights are optimized similar to [9]. At the RX side, any type of RF beamforming weights can be used, i.e., either directional or omnidirectional beam patterns. However, here they are designed to maximize the gain at the angle corresponding to the sensing beam θ_{r}, providing a directional beam pattern.

B. MIMO Radar

Assuming there are K_{t} point targets, the TX signal is reflected from these and received back at the radar RX as

$$\tilde{\mathbf{y}}_{n,m} = \sum_{k=1}^{K_{\text{t}}} b_k e^{-\jmath 2\pi n \Delta f \tau_k} \mathbf{a}_{\text{R}}(\theta_k) \mathbf{a}_{\text{T}}^{H}(\theta_k) \tilde{\mathbf{x}}_{n,m} + \tilde{\mathbf{v}}_{n,m}, \tag{4}$$

where $\tilde{\mathbf{y}}_{n,m}$ and $\tilde{\mathbf{v}}_{n,m}$ are the RX frequency-domain symbol vector and the noise sample vector, respectively, of sizes $L_{\text{R}} \times 1$. The variables b_k and τ_k denote the attenuation constant and two-way delay of the k^{th} target, while $\mathbf{a}_{\text{R}}(\theta_k)$ and $\mathbf{a}_{\text{T}}(\theta_k)$ are the RX and TX steering vectors corresponding to the same target. The subcarrier spacing is denoted by Δf. Additionally, angles of departure and arrival, expressed by θ_k, are considered to be the same, assuming far targets and the TX and RX arrays being closely situated. For a uniform linear array with half-wavelength separation between the L antenna elements, the steering vector for a general angle θ is given by

$$\mathbf{a}(\theta) = \left[1, e^{\jmath\pi \sin(\theta)}, \ldots, e^{\jmath\pi(L-1)\sin(\theta)}\right]^{T}. \tag{5}$$

Converting (4) into a matrix notation yields

$$\tilde{\mathbf{y}}_{n,m} = \mathbf{A}_{\text{R}}(\boldsymbol{\theta}) \mathbf{H}_{\text{rad},n} \mathbf{A}_{\text{T}}^{H}(\boldsymbol{\theta}) \tilde{\mathbf{x}}_{n,m} + \tilde{\mathbf{v}}_{n,m}, \tag{6}$$

where $\mathbf{A}_{\text{R}}(\boldsymbol{\theta}) = [\mathbf{a}_{\text{R}}(\theta_1), \ldots, \mathbf{a}_{\text{R}}(\theta_{K_{\text{t}}})]$ is of size $L_{\text{R}} \times K_{\text{t}}$ and $\mathbf{A}_{\text{T}}(\boldsymbol{\theta}) = [\mathbf{a}_{\text{T}}(\theta_1), \ldots, \mathbf{a}_{\text{T}}(\theta_{K_{\text{t}}})]$ is of size $L_{\text{T}} \times K_{\text{t}}$, and they contain the steering vectors for all the targets. Additionally, $\boldsymbol{\theta} = [\theta_1, \ldots, \theta_{K_{\text{t}}}]^{T}$ is the vector of all targets' directions. The diagonal matrix $\mathbf{H}_{\text{rad},n}$ is of size $K_{\text{t}} \times K_{\text{t}}$, and it represents the radar channel where $(\mathbf{H}_{\text{rad},n})_{k,k} = b_k e^{-\jmath 2\pi n \Delta f \tau_k}$. Then, the RX BB frequency-domain symbols are given by

$$\begin{aligned} \mathbf{y}_{n,m} &= (\mathbf{W}_{\text{R}}^{\text{RF}})^{H} \tilde{\mathbf{y}}_{n,m} \\ &= \underbrace{(\mathbf{W}_{\text{R}}^{\text{RF}})^{H} \mathbf{A}_{\text{R}}(\boldsymbol{\theta}) \mathbf{H}_{\text{rad},n} \mathbf{A}_{\text{T}}^{H}(\boldsymbol{\theta}) \mathbf{W}_{\text{T}}^{\text{RF}} \mathbf{W}_{\text{T}}^{\text{BB}}}_{\mathbf{H}_n} \mathbf{x}_{n,m} + \mathbf{v}_{n,m}, \end{aligned} \tag{7}$$

where the RX RF combiner $\mathbf{W}_{\text{R}}^{\text{RF}}$ is of size $L_{\text{R}} \times L_{\text{R}}^{\text{RF}}$ and $\mathbf{y}_{n,m}$ is a vector of size $L_{\text{R}}^{\text{RF}} \times 1$. The effective channel between the TX streams and the RX BB symbols is given by $\mathbf{H}_n$, which is of size $L_{\text{R}}^{\text{RF}} \times (S \cdot U)$.

Assuming $\mathbf{H}_n$ to be a time-invariant channel for different OFDM symbols, (7) can alternatively be written by stacking for different OFDM symbols as

$$\underbrace{\begin{bmatrix} \mathbf{y}_{n,1} \\ \mathbf{y}_{n,2} \\ \vdots \\ \mathbf{y}_{n,M} \end{bmatrix}}_{\mathbf{y}_n} = \underbrace{\begin{bmatrix} x_{n,1,1}\mathbf{I} & \ldots & x_{n,1,S\cdot U}\mathbf{I} \\ x_{n,2,1}\mathbf{I} & \ldots & x_{n,2,S\cdot U}\mathbf{I} \\ \vdots & \vdots & \vdots \\ x_{n,M,1}\mathbf{I} & \ldots & x_{n,M,S\cdot U}\mathbf{I} \end{bmatrix}}_{\mathbf{X}_n} \underbrace{\begin{bmatrix} \mathbf{h}_{n,1} \\ \mathbf{h}_{n,2} \\ \vdots \\ \mathbf{h}_{n,S\cdot U} \end{bmatrix}}_{\mathbf{h}_n} + \mathbf{v}_n, \tag{8}$$

where $x_{n,m,s} = (\mathbf{x}_{n,m})_s$ for $s \in [1, S \cdot U]$ denotes the s^{th} element of $\mathbf{x}_{n,m}$ and $\mathbf{h}_{n,s} = (\mathbf{H}_n)_s$ denotes the s^{th} column of $\mathbf{H}_n$. Here, $\mathbf{I}$ is the $L_{\text{R}}^{\text{RF}} \times L_{\text{R}}^{\text{RF}}$ identity matrix, and $\mathbf{y}_n$, $\mathbf{X}_n$, $\mathbf{h}_n$ and $\mathbf{v}_n$ are of dimensions $(L_{\text{R}}^{\text{RF}} \cdot M) \times 1$, $(L_{\text{R}}^{\text{RF}} \cdot M) \times (S \cdot U \cdot L_{\text{R}}^{\text{RF}})$, $(S \cdot U \cdot L_{\text{R}}^{\text{RF}}) \times 1$, and $(L_{\text{R}}^{\text{RF}} \cdot M) \times 1$, respectively.

III. Range–Angle Processing

This section showcases the procedure adopted in obtaining the range–angle map corresponding to the targets. In this paper, we build upon the work done in [9], where range and angle profiles were calculated separately from the RX BB symbols. Due to this reason, ranges and angles of the targets were not associated with each other. However in this work, the calculated range profiles are subsequently used to calculate the angle profiles. Hence, the targets' ranges can be associated with the corresponding angles. This is the main difference compared to [9], while here we also extensively discuss the processing involved.

The objective of radar processing is to estimate targets' delays and angles, which can be done by estimating $\mathbf{h}_n$ as

$$\hat{\mathbf{h}}_n = \begin{bmatrix} \hat{\mathbf{h}}_{n,1} \\ \hat{\mathbf{h}}_{n,2} \\ \vdots \\ \hat{\mathbf{h}}_{n,S\cdot U} \end{bmatrix} = \mathbf{X}_n^{\dagger} \mathbf{y}_n = \mathbf{h}_n + \bar{\mathbf{h}}_n, \tag{9}$$

where $\hat{\mathbf{h}}_n$ is the estimate for $\mathbf{h}_n$, $\bar{\mathbf{h}}_n$ is the estimation error vector and $(\cdot)^\dagger$ is the pseudo-inverse operation. When sufficient number of OFDM symbols is used, $\mathbf{X}_n$ can be assumed to have full rank, i.e., it is quite unlikely that different OFDM symbols carry the same stream of frequency-domain symbols. In this case, the matrix $\mathbf{X}_n^H\mathbf{X}_n$ will also be of full rank. Hence, the inverse of that matrix, i.e., $(\mathbf{X}_n^H\mathbf{X}_n)^{-1}$, exists, and therefore the pseudo-inverse is given by $\mathbf{X}_n^\dagger = (\mathbf{X}_n^H\mathbf{X}_n)^{-1}\mathbf{X}_n^H$.

A. Calculation of the Range Profiles

For the s^{th} TX stream, L_{R}^{RF} different values can be calculated for the i^{th} range bin by applying the inverse discrete Fourier transform (IDFT) to $\hat{\mathbf{h}}_{n,s}$, similar to the scalar case in [10] as

$$\mathbf{d}_{i,s} = \sum_{n=1}^{N} q_{i,n}\hat{\mathbf{h}}_{n,s} = \left[\hat{\mathbf{h}}_{1,s},\ldots,\hat{\mathbf{h}}_{N,s}\right]\mathbf{q}_i, \tag{10}$$

where $i \in [1, N]$ and $\mathbf{q}_i$ is the IDFT vector of size $N \times 1$, and each element of it is given by $(\mathbf{q}_i)_n = q_{i,n} = e^{\frac{j2\pi ni}{N}}$, while $\mathbf{d}_{i,s}$ is a vector of size $L_{\text{R}}^{\text{RF}} \times 1$. Although $\mathbf{d}_{i,s}$ depends on $\boldsymbol{\theta}$, it is not shown explicitly for simplicity of notation. The delay of each target is discretized as $\tau_i = \frac{i}{N\Delta f}$.

Since there are L_{R}^{RF} different range bin values for the s^{th} stream, they can be combined at the radar RX to yield a single value. The angle-dependent complex coefficient of the RX beam pattern at a particular direction θ, including also the BB weights at the RX is given as

$$g_{\text{R}}(\theta) = (\mathbf{w}_{\text{R}}^{\text{BB}}(\theta))^H(\mathbf{W}_{\text{R}}^{\text{RF}})^H\mathbf{a}_{\text{R}}(\theta), \tag{11}$$

where $\mathbf{w}_{\text{R}}^{\text{BB}}(\theta)$ is of size $L_{\text{R}}^{\text{RF}} \times 1$. Then, the RX BB weights that maximize $g_{\text{R}}(\theta)$ under the constraint $\|\mathbf{w}_{\text{R}}^{\text{BB}}(\theta)\| = 1$ (unit norm), are given by the solution for the spatial matched-filter (MF) as

$$\mathbf{w}_{\text{R}}^{\text{BB}}(\theta) = \frac{(\mathbf{W}_{\text{R}}^{\text{RF}})^H\mathbf{a}_{\text{R}}(\theta)}{\|(\mathbf{W}_{\text{R}}^{\text{RF}})^H\mathbf{a}_{\text{R}}(\theta)\|}. \tag{12}$$

Then, the single value for the i^{th} range bin and for the s^{th} TX stream is given by $(\mathbf{w}_{\text{R}}^{\text{BB}}(\theta))^H\mathbf{d}_{i,s}$, and performing this for all the streams, they can be stacked into a vector as

$$\mathbf{d}_i = [(\mathbf{w}_{\text{R}}^{\text{BB}}(\theta))^H\mathbf{d}_{i,1},\ldots,(\mathbf{w}_{\text{R}}^{\text{BB}}(\theta))^H\mathbf{d}_{i,S\cdot U}]^T, \tag{13}$$

where $\mathbf{d}_i$ is of size $(S \cdot U) \times 1$.

B. Calculation of the Angle Profiles

For calculating the angle profiles, the covariance matrix of the range bin values across different RF chains is needed. Hence, this will be first calculated based on (10). Adopting (9), $\hat{\mathbf{h}}_{n,s} = \mathbf{h}_{n,s} + \bar{\mathbf{h}}_{n,s}$, where $\bar{\mathbf{h}}_{n,s}$ is the corresponding estimation error vector, the covariance matrix of the i^{th} range bin is then given by

$$\begin{aligned}\mathbf{R}_{\mathbf{d},i,s} &= \mathbb{E}\{\mathbf{d}_{i,s}\mathbf{d}_{i,s}^H\} \\ &= \mathbb{E}\left\{\left(\sum_{n_1=1}^{N} q_{i,n_1}\hat{\mathbf{h}}_{n_1,s}\right)\left(\sum_{n_2=1}^{N} q_{i,n_2}^*\hat{\mathbf{h}}_{n_2,s}^H\right)\right\} \\ &= \sum_{n_1=1}^{N}\sum_{n_2=1}^{N} q_{i,n_1}q_{i,n_2}^*\mathbf{h}_{n_1,s}\mathbf{h}_{n_2,s}^H + \sigma^2\mathbf{I}. \end{aligned}\tag{14}$$

Here, the expectation operation is denoted by $\mathbb{E}\{\cdot\}$ and the covariance matrix of the estimation error is given by $\sigma^2\mathbf{I} = \sum_{n_1=1}^{N}\sum_{n_2=1}^{N} q_{i,n_1}q_{i,n_2}^*\mathbb{E}\{\bar{\mathbf{h}}_{n_1,s}\bar{\mathbf{h}}_{n_2,s}^H\}$. Since $\mathbf{h}_{n,s}$ corresponds to $(\mathbf{H}_n)_s = (\mathbf{W}_{\text{R}}^{\text{RF}})^H\mathbf{A}_{\text{R}}(\boldsymbol{\theta})\mathbf{H}_{\text{rad},n}\mathbf{A}_{\text{T}}^H(\boldsymbol{\theta})\mathbf{W}_{\text{T}}^{\text{RF}}(\mathbf{W}_{\text{T}}^{\text{BB}})_s$, (14) can be rewritten as

$$\mathbf{R}_{\mathbf{d},i,s} = \mathbf{A}_{\text{RF}}(\boldsymbol{\theta})\mathbf{R}_{\text{res},i,s}\mathbf{A}_{\text{RF}}^H(\boldsymbol{\theta}) + \sigma^2\mathbf{I}, \tag{15}$$

where $\mathbf{A}_{\text{RF}}(\boldsymbol{\theta}) = (\mathbf{W}_{\text{R}}^{\text{RF}})^H\mathbf{A}_{\text{R}}(\boldsymbol{\theta})$ is of size $L_{\text{R}}^{\text{RF}} \times K_{\text{t}}$ and

$$\begin{aligned}\mathbf{R}_{\text{res},i,s} = \sum_{n_1=1}^{N}\sum_{n_2=1}^{N} q_{i,n_1}q_{i,n_2}^*(\mathbf{H}_{\text{rad},n_1}\mathbf{A}_{\text{T}}^H(\boldsymbol{\theta})\mathbf{W}_{\text{T}}^{\text{RF}}(\mathbf{W}_{\text{T}}^{\text{BB}})_s) \\ \cdot(\mathbf{H}_{\text{rad},n_2}\mathbf{A}_{\text{T}}^H(\boldsymbol{\theta})\mathbf{W}_{\text{T}}^{\text{RF}}(\mathbf{W}_{\text{T}}^{\text{BB}})_s)^H\end{aligned}\tag{16}$$

is the covariance matrix due to the residual terms apart from $\mathbf{A}_{\text{RF}}(\boldsymbol{\theta})$ in $(\mathbf{H}_n)_s$. In practice, an approximation is used for the covariance matrix in (14), given by $\mathbf{R}_{\mathbf{d},i,s} \approx \mathbf{d}_{i,s}\mathbf{d}_{i,s}^H$.

The first term on the right-side in (15) will have $(L_{\text{R}}^{\text{RF}} - K_{\text{t}})$ zero eigenvalues, where each corresponding eigenvector is represented by $\boldsymbol{\gamma}_p$, of size $L_{\text{R}}^{\text{RF}} \times 1$, with $p \in [1, L_{\text{R}}^{\text{RF}} - K_{\text{t}}]$. Each of them should obey $\mathbf{A}_{\text{RF}}(\boldsymbol{\theta})\mathbf{R}_{\text{res},i,s}\mathbf{A}_{\text{RF}}^H(\boldsymbol{\theta})\boldsymbol{\gamma}_p = \mathbf{0}$, where the zero vector is denoted by $\mathbf{0}$. After some simplification, the solution can be given as $\mathbf{A}_{\text{RF}}^H(\boldsymbol{\theta})\boldsymbol{\gamma}_p = \mathbf{A}_{\text{R}}^H(\boldsymbol{\theta})\mathbf{W}_{\text{R}}^{\text{RF}}\boldsymbol{\gamma}_p = \mathbf{0}$. Then, it can be shown that the eigenvectors of $\mathbf{R}_{\mathbf{d},i,s}$ corresponding to the $(L_{\text{R}}^{\text{RF}} - K_{\text{t}})$ lowest eigenvalues are the same as $\boldsymbol{\gamma}_p$. Hence, to find the angle profile, eigendecomposition of $\mathbf{R}_{\mathbf{d},i,s}$ is first performed to find $\boldsymbol{\gamma}_p$ to write the MUSIC pseudo-spectrum of the i^{th} range bin and s^{th} stream as [9]

$$P(\theta)_{i,s} = \frac{1}{\tilde{\mathbf{a}}^H(\theta)\boldsymbol{\Gamma}_{i,s}\boldsymbol{\Gamma}_{i,s}^H\tilde{\mathbf{a}}(\theta)}, \tag{17}$$

where $\boldsymbol{\Gamma}_{i,s} = [\boldsymbol{\gamma}_{i,s,1},\ldots,\boldsymbol{\gamma}_{i,s,L_{\text{R}}^{\text{RF}}-K_{\text{t}}}]$ is the matrix containing eigenvectors corresponding to the zero eigenvalues, $\theta \in [-90°, 90°]$, and $\tilde{\mathbf{a}}(\theta) = (\mathbf{W}_{\text{R}}^{\text{RF}})^H\mathbf{a}_{\text{R}}(\theta)$. This is performed for all the range bins to obtain the range–angle map corresponding to each TX stream.

The complexity of range–angle processing depends mainly on three operations: the pseudo-inverse in (9), the IDFT in (10), and the eigendecomposition of $\mathbf{R}_{\mathbf{d},i,s}$ in (14), respectively. The computational complexity of all these operations depends on the dimensions of the corresponding matrices, i.e., M, N, S, U, and L_{R}^{RF}. Generally, N is the highest value out of these, and thus a higher value for it increases the computational complexity, while simultaneously improving the range resolution, indicating its trade-off.

C. Combination of Range and Angle Profiles

As observed from (17), $S \cdot U$ TX streams will produce that many different angle profiles for the i^{th} range bin, and hence different range–angle maps. This is due to $\mathbf{W}_{\text{T}}^{\text{BB}}$ having disparate weights for the TX streams. However, in the perspective of radar processing, a single range–angle map is required, which can be performed through maximum-ratio combining. For the s^{th} TX stream, the angle-dependent complex coefficient of the beam pattern is given as

$$g_{\text{T},s}(\theta) = \mathbf{a}_T^H(\theta)\mathbf{W}_{\text{T}}^{\text{RF}}(\mathbf{W}_{\text{T}}^{\text{BB}})_s, \tag{18}$$

and thus the combined MUSIC pseudo-spectrum can be written for the i^{th} range bin as

$$P(\theta)_i = \sum_{s=1}^{S\cdot U} |g_{\text{T},s}(\theta)|^2 P(\theta)_{i,s} = \sum_{s=1}^{S\cdot U} \frac{|g_{\text{T},s}(\theta)|^2}{\tilde{\mathbf{a}}^H(\theta)\mathbf{\Gamma}_{i,s}\mathbf{\Gamma}_{i,s}^H\tilde{\mathbf{a}}(\theta)}. \quad (19)$$

Finally, a similar approach could be applied to $\mathbf{d}_i$ in (13) to obtain a single range bin value as

$$d_{\text{comb},i} = \sum_{s=1}^{S\cdot U} g_{\text{T},s}^*(\theta_\text{r})(\mathbf{d}_i)_s, \quad (20)$$

where $g_{\text{T},s}^*(\theta_\text{r})$ is used to coherently combine the different range bin values computed for different TX streams.

IV. Numerical Results

In this section, the proposed range–angle processing is simulated for the considered MIMO hybrid architecture. The parameters used for the simulations are $L_\text{T} = L_\text{R} = 32$, $L_\text{T}^\text{RF} = L_\text{R}^\text{RF} = 8$, $U = 2$, $S = 1$, $M = 10$, $N = 3168$, $\Delta f = 120$ kHz, and a signal-to-noise ratio of 30 dB at the radar RX. It should be noted that the processing still works for $S > 1$, but for simplicity we consider $S = 1$. Additionally, the TX and RX antenna arrays are simulated with CST Studio Suite to observe the performance with realistic antennas.

Three beams are used in the TX at angles $\theta_\text{r} = 10°$, $\theta_{\text{c},1} = -40°$ and $\theta_{\text{c},2} = 30°$, where only the first user's stream is transmitted at $\theta_{\text{c},1}$, while the second user's stream is only transmitted at $\theta_{\text{c},2}$. However, both streams are transmitted to θ_r. Additionally, for the first user's TX beam pattern, a null is imposed at $\theta_{\text{c},2}$, while for the second user's beam pattern, that null is at $\theta_{\text{c},1}$, to cancel the inter-user interference between the two users. All these requirements are performed by optimizing $\mathbf{W}_\text{T}^\text{BB}$ and $\mathbf{W}_\text{T}^\text{RF}$, similar to [9]. Then at the RX side, a single beam is used at θ_r, obtained by optimizing $\mathbf{W}_\text{R}^\text{RF}$. Six point targets with a radar cross section of $50\ m^2$ are placed as depicted in Fig. 2(a). Targets that have almost the same angle are grouped together as depicted in the figure. Here, $\theta_\text{oth} \approx 19°$, and it denotes the angle where there is some clutter, separate from the communication users and the sensing target.

Figure 2(b) depicts the range profiles for the considered scenario, where a single range profile is obtained per each TX stream using (11)–(13). For the first user's stream transmitted at $\theta_{\text{c},1}$, the target at $\theta_{\text{c},2}$ is not observed, while those at $\theta_{\text{c},1}$ are not observed with the second user's TX stream at $\theta_{\text{c},2}$. This is because the TX beam pattern corresponding to one user has a null at the other user's direction to mitigate the inter-user interference [9]. Then, the radar target at θ_r is observed by the two TX streams since they both are transmitted at that angle. Although there are two targets at θ_oth, only a single target is observed by both TX streams since the range resolution is not high enough to differentiate between them. The figure also shows the single range profile obtained by combining the range profiles corresponding to the two TX streams using (20).

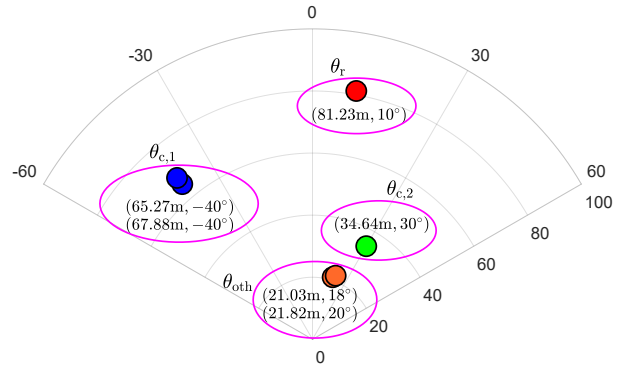

(a) Target scenario

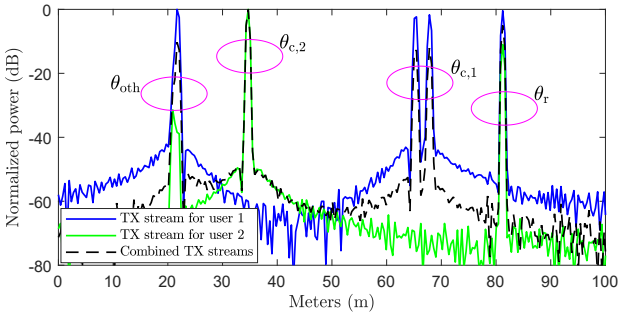

(b) The range profiles obtained for the different TX streams

Fig. 2. The considered target scenario and the corresponding range profiles obtained for the different TX streams.

Then, Figs. 3(a)–(c) show the 3D range–angle maps using a MF approach, whereas Figs. 3(d)–(f) are with the MUSIC approach. In both approaches, the three figures are with the first TX stream, second stream, and both streams combined, respectively. In the MF approach, the L_R^RF different range profiles for the s^{th} TX stream are combined for a particular angle θ using (11)–(13). Performing this for $\theta \in [-90°, 90°]$, the corresponding range–angle map is found, and the single range–angle map can be obtained using (19).

Figures 3(a)–(b) show that although the targets' ranges can be clearly distinguished, there are ambiguities in the angles. This is because of the grating lobes in the effective pattern of each subarray (combination of RF and BB), due to the distance between them being more than a half-wavelength separation. Figure 3(c) then depicts the combined range–angle map for all the targets. Despite of the ambiguities, the combination has reduced the noise level of the range–angle map.

In the MUSIC approach, combination of different range profiles are done similarly with (11)–(13), but only for the sensing direction θ_r, while range–angle maps are combined with (19). The ambiguities in the angles are quite weak with this approach, as illustrated in Figs. 3(d)–(e). Moreover, the target(s) at the second/first user's direction is(/are) not observed by the first/second TX stream, as in Fig. 2(b), while the target at θ_r is observed by both. Then, combining the two streams allows to cancel the ambiguities well, distinguishing between all the targets, as shown in Fig. 3(f).

The two closely situated targets at θ_oth can now be observed, which are not seen in Fig. 2(b), indicating the super-resolution

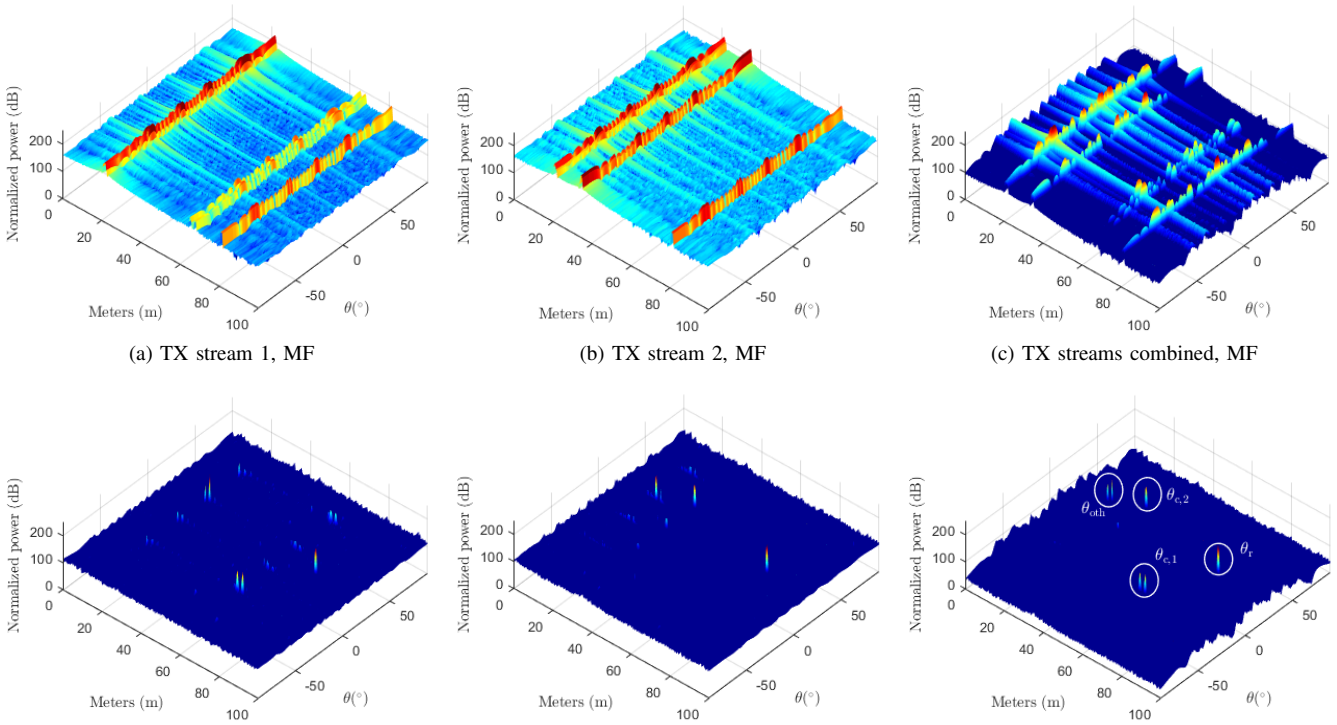

(a) TX stream 1, MF (b) TX stream 2, MF (c) TX streams combined, MF

(d) TX stream 1, MUSIC (e) TX stream 2, MUSIC (f) TX streams combined, MUSIC

Fig. 3. The range–angle maps corresponding to the considered scenario, using the MF and MUSIC approaches, where (f) also shows the targets in Fig. 2(a).

provided in the angular domain. Comparing the range–angle map in Fig. 3(f) with the one obtained in [5], it can be observed that the proposed processing scheme works quite well similar to that of a MIMO radar. Additionally, although a single RX beam is used at the sensing direction, the range–angle map also shows targets from other directions. This provides more information for the communication system which can use that to better cater to its users. Once the range–angle map is obtained, any detection scheme can be applied afterwards.

V. Conclusion

The sensing signal processing involved with obtaining the range–angle map is discussed here for a hybrid MIMO JCAS system employing OFDM. At the TX side, multiple beams are used to cater to different communication users, while an additional beam is used to sense the environment. Then, at the MIMO RX, different users' TX streams are used to obtain the range profiles corresponding to the targets in the environment, and they are subsequently utilized to derive the angle profiles using the MUSIC algorithm. The simulations indicate that it performs better than the spatial MF, while even targets situated very close in the angular domain can be reliably observed owing to the super-resolution of the MIMO processing.

Acknowledgment

This research was partially supported by the Academy of Finland (grants #315858, #319994, #328214, and #341489), Nokia Bell Labs, and the Doctoral School of Tampere University. This research was also supported by the Finnish Funding Agency for Innovation through the "RF Convergence" project.

References

[1] B. Paul, A. R. Chiriyath, and D. W. Bliss, "Survey of RF communications and sensing convergence research," *IEEE Access*, vol. 5, pp. 252–270, 2017.

[2] C. Baquero Barneto, S. D. Liyanaarachchi, M. Heino, T. Riihonen, and M. Valkama, "Full-duplex radio/radar technology: The enabler for advanced joint communication and sensing," *IEEE Wireless Communications*, Feb. 2021.

[3] S. A. Busari, K. M. S. Huq, S. Mumtaz, L. Dai, and J. Rodriguez, "Millimeter-wave massive MIMO communication for future wireless systems: A survey," *IEEE Communications Surveys Tutorials*, vol. 20, no. 2, pp. 836–869, Dec. 2017.

[4] L. Xu, J. Li, and P. Stoica, "Target detection and parameter estimation for MIMO radar systems," *IEEE Transactions on Aerospace and Electronic Systems*, vol. 44, no. 3, pp. 927–939, Oct. 2008.

[5] Y. L. Sit, C. Sturm, J. Baier, and T. Zwick, "Direction of arrival estimation using the MUSIC algorithm for a MIMO OFDM radar," in *Proc. IEEE Radar Conference*, May 2012, pp. 226–229.

[6] F. Liu, C. Masouros, A. Li, H. Sun, and L. Hanzo, "MU-MIMO communications with MIMO radar: From co-existence to joint transmission," *IEEE Trans. Wireless Commun.*, vol. 17, no. 4, pp. 2755–2770, Apr. 2018.

[7] X. Gao, L. Dai, S. Han, C. I, and R. W. Heath, "Energy-efficient hybrid analog and digital precoding for mmwave MIMO systems with large antenna arrays," *IEEE Journal on Selected Areas in Communications*, vol. 34, no. 4, pp. 998–1009, Apr. 2016.

[8] X. Zhang, L. Xu, L. Xu, and D. Xu, "Direction of departure (DOD) and direction of arrival (DOA) estimation in MIMO radar with reduced-dimension MUSIC," *IEEE Communications Letters*, vol. 14, no. 12, pp. 1161–1163, Nov. 2010.

[9] S. D. Liyanaarachchi, C. Baquero Barneto, T. Riihonen, M. Heino, and M. Valkama, "Joint multi-user communication and MIMO radar through full-duplex hybrid beamforming," in *Proc. IEEE International Online Symposium on Joint Communications & Sensing*, Feb. 2021.

[10] S. D. Liyanaarachchi, C. Baquero Barneto, T. Riihonen, and M. Valkama, "Joint OFDM waveform design for communications and sensing convergence," in *Proc. IEEE Int. Conf. on Commun.*, Jun. 2020.